International Journal of Fracture **85:** 313–331, 1997.

Theoretical simulations of a propagating crack subjected to in-plane stress wave loading by caustic method

YI-SHYONG ING* and CHIEN-CHING MA**
Department of Mechanical Engineering, National Taiwan University, Taipei, Taiwan 10617, Republic of China

Received 30 December 1996; accepted in revised form 2 July 1997

Abstract. The optical method of caustics for measuring the dynamic stress intensity factor in a transient process is investigated in this study. The transient full-field solutions of a propagating crack contained in an infinite medium subjected to step-stress wave and ramp-stress wave loadings are used to establish the exact equations of the initial and caustic curves. The results of the stress intensity factor obtained from the caustic method are compared with theoretical predictions and some experiments. The results demonstrate that a significant deviation can occur in the determination of the dynamic stress intensity factor from shadow spot measurements. The factors, such as screen distance, magnitude of loading, crack speed and rising time which can influence the accuracy of the experimental measurements are discussed in detail. In addition, the valid region of the dynamic stress singular field for the propagating crack is discussed in detail and it gives a better understanding of the appropriate region of measurements for investigators.

Key words: Caustic method, Stress intensity factor, Stress wave, Crack propagation.

1. Introduction

In fracture mechanics, the idea of the stress intensity factor of a cracked body is well established and the measurement of the stress intensity factor becomes the major work of relative experiments. Several experimental methods, such as photoelasticity, interferometry and caustics were developed to determine such factors. The optical method of caustics, a technique based on geometrical optics, has been successfully applied to the study of deformation fields in solids. It has several advantages over the other optical methods due to its simplicity. The method of caustics requires less equipment and a simple optical set-up, and it can be applied to the investigation of both transparent or opaque materials. Therefore, it has been widely used in many applications of fracture mechanics, especially in the measurement of static and dynamic stress intensity factors.

The method of caustics was initially introduced by Schardin (1959) and Manogg (1964) was the first person who showed that the geometrical characteristics of the caustic depend on the intensity of the crack tip singularity and was able to measure the intensity of the near-tip stress field. Theocaris (1971) used the method in a reflection arrangement, and subsequently Theocaris and Gdoutos (1974) applied this method to examine the deformation fields near a stationary crack tip. In the late 1970s, the method of caustics has been developed into a standard and efficient technique for measurement of the static and dynamic fracture toughnesses of elastic materials. Rosakis (1980) provided analyses to account for the effects of material inertia in the interpretation of caustic data obtained with light reflected from specimens of opaque materials. In a paper by Rosakis et al. (1983), the method of caustics for a power-law

* Graduate Student.
** Professor and author for correspondence.

hardening material in a state of plane stress was established, and a relationship between the value of Rice's J integral and the maximum transverse diameter of the shadow spot was derived.

The caustic method mentioned above is based on the fact that the value of the stress intensity factor can be related to features of the optical field obtained by directing parallel light through a transparent specimen in the crack tip region, or by reflecting light from the surface of an opaque specimen in the crack tip region. There are assumptions in deriving the method of caustics, hence the formula of the caustic used in determining the stress intensity factor is subjected to some restrictions. In deriving the formula of the caustic, several assumptions are made

(a) the specimen is in a plane stress state;
(b) the deformation slope is small;
(c) small scale yielding prevails;
(d) the measurements are made within the region of dominant singular field.

Hence, the caustic method should be performed under those conditions to get good experimental results. These assumptions have been carried through in most of the subsequent applications of caustics. It is only recently that those restrictions have been investigated and some conclusions have been made to improve the validity and accuracy of caustic methods. Rosakis and Ravi-Chandar (1986) analyzed the limitation of the plane stress interpretation of caustics data on compact tension specimens. The results indicated that plane stress conditions prevail at distances from the crack tip greater than half the specimen thickness. Plasticity at the crack tip also limits the minimum distance from the tip where optical measurements can be performed. Analysis by Rosakis and Freund (1981) has shown that the error introduced through the neglect of plasticity effects in the interpretation of caustics data will be small as long as the measurement is performed in a radius greater than twice the plastic zone size. The implicit assumptions of the usual small angle reflection in the evaluation of stress intensity factors by shadow spot measurements are discussed in detail by Rosakis and Zehnder (1985). The exact equations were derived for caustics formed by the reflection of light from a general surface, the results demonstrated significant deviation from the approximate analyses resulting in errors as large as 15 percent in the determination of the stress intensity factor.

Recently, many experimental results and investigations, such as Freund and Rosakis (1992) and Krishnaswamy and Rosakis (1991), indicated that the assumption of K dominance is not always adequate to describe the deformed behavior in the vicinity of a propagating crack tip. In order to explain the phenomena of experiments, Ma (1990) has used the exact solutions of static crack and the transient stress field of a stationary crack subjected to dynamic loading to simulate the experiment of caustics. He has found that very accurate measurement of the stress intensity factor by caustic methods can be obtained only if the initial curves are within one tenth of the crack length for static loading and one tenth of the longitudinal wave front for dynamic loading. Aoki and Kimura (1993) used two- and three-dimensional finite element methods to investigate the experiment of caustics for a propagating crack. They declared that the dynamic stress intensity factor depends on the incident wave form and also on the loading rate for a short time-to-fracture. Based on the higher order transient expansion obtained by Freund and Rosakis (1990), Liu et al. (1993) established an explicit relation between the instantaneous value of the dynamic stress intensity factor and the geometrical characteristics of the caustic. They also used the Broberg problem as an example problem to compare the difference between the classical analysis and the improved method proposed by them. Recalling the assumptions

(a), (b), (c) and (d) as indicated above, the points at which experimental data are taken can not be too close to the crack tip because of the restriction of the plane stress state, plastic zone effect and small slope of the deformed surface. The points can not be too far away from the crack tip either, because of the K dominance assumption. Hence, the region which is suitable for the experimental measurement is an annular zone surrounding the crack tip. In this study, we try to give some information on the determination of the outer boundary for satisfactory accuracy of the stress intensity factor measurement by using the caustic method.

In this paper, the exact transient solutions of a propagating crack subjected to step-stress and ramp-stress wave loadings are used to establish the exact equations of the caustic envelope. The validity of the stress singular field is also investigated to determine the appropriate region for measurements with acceptable accuracy by the method of caustics. The experimental results of Ravi-Chandar and Knauss (1984a,b,c,d) are used for comparison with the simulating analysis for the stationary crack. The factors that influenced the accuracy of the experimental measurement are discussed in detail. Furthermore, the ratio of the exact full-field transient stress to the stress singular field is computed numerically so that the valid region of the stress singular field in the transient process can be investigated more accurately.

2. Formation of caustic in reflection

Consider a highly polished planar specimen of uniform thickness h in the undeformed state occupying a region in the x–y plane. If the plate is subjected to an external loading, the resulting change thickness in terms of the in-plane stress components is given by

$$f(x,y) = -w(x,y) = \frac{\sigma h}{2E}(\tau_{xx} + \tau_{yy}), \tag{1}$$

where σ is the Poisson's ratio, E is the Young's elastic modulus and w is the displacement in the thickness direction.

Consider a family of light rays travelling in the z-direction, normally incident on the reflecting surface as illustrated in Figure 1. Upon passing through the specimen, the direction of each ray is modified. The amount of deviation for each ray depends on local conditions, in particular, on the local thinning of the specimen due to in-plane stress. If certain geometrical conditions are met by the reflecting surface, then the extensions of the reflected rays will form an envelope of a three-dimensional surface in space. This surface, which is called the caustic surface, is the locus of points of maximum luminosity in the reflected light field. A screen is positioned parallel to the x–y plane so that it intersects the caustic surface at a distance z_0 from the undeformed specimen. Under suitable conditions, the light field on the screen will appear as a dark spot (the shadow spot) surrounded by a bright border (the caustic curve), with diminishing light intensity away from the caustic curve. If the plane of the specimen is the x–y plane, then let the X–Y plane be the plane of the screen, where the screen coordinate axes are obtained by translating the specimen coordinate axis in the directional normal to the specimen. The position of the image point on the screen will depend on the slope of the reflecting surface and on the normal distance z_0, the light ray which strikes the specimen at point (x, y) then strikes the screen at the point (X, Y), and the optical mapping may be written as (Rosakis et al., 1983)

$$X = x - 2(z_0 - f)\frac{\partial f/\partial x}{1 - (\partial f/\partial x)^2 - (\partial f/\partial y)^2}, \tag{2}$$

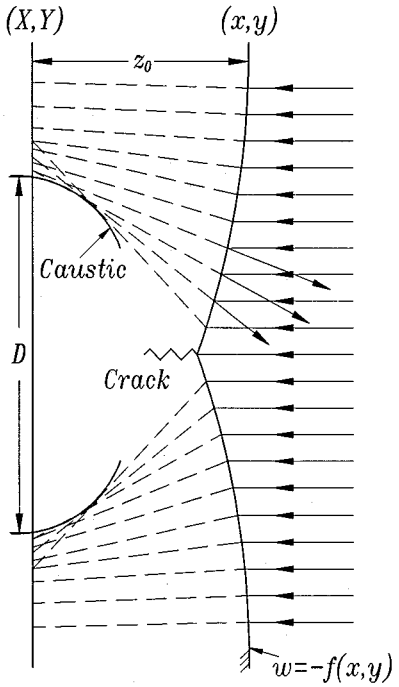

Figure 1. Schematic diagram of the optical reflection process and the formation of a caustic envelope.

$$Y = y - 2(z_0 - f)\frac{\partial f/\partial y}{1 - (\partial f/\partial x)^2 - (\partial f/\partial y)^2}. \tag{3}$$

If it is now assumed that $|f| \ll z_0$ and that $(\partial f/\partial x)^2 + (\partial f/\partial y)^2 \ll 1$, which is usually the case in most practical applications, then the optical mapping simplifies to

$$X = x - 2z_0 \partial f/\partial x, \tag{4}$$

$$Y = y - 2z_0 \partial f/\partial y. \tag{5}$$

If the screen intersects a caustic surface in the reflected light field, then the resulting caustic curve on the screen is a locus of points for which the mapping described by (4) and (5) is not invertible and the determinant of the Jacobian matrix of the mapping must vanish, i.e.

$$\frac{\partial(X,Y)}{\partial(x,y)} = 1 - 2z_0\left(\frac{\partial^2 f}{\partial x^2} + \frac{\partial^2 f}{\partial y^2}\right) - 4z_0^2\left[\left(\frac{\partial^2 f}{\partial x \partial y}\right)^2 - \frac{\partial^2 f}{\partial x^2}\frac{\partial^2 f}{\partial y^2}\right] = 0. \tag{6}$$

The points on the plane of the undeformed reflecting surface for which the Jacobian determinant vanishes are the points from which the rays forming the caustic curve are reflected. The locus of these points on the reflecting surface is the so-called initial curve. In other words, the curve on the specimen which maps into the caustic curve according to (4) and (5) is the initial curve. The light rays which strike the specimen both inside and outside of the initial curve map into points on the screen which are outside of the caustic curve. Since the interpretation of the stress field at the crack tip in terms of the stress intensity factor is

appropriate only in a very small region around the crack tip, the reliability of the method of caustics depends on the size of the initial curve. This property gives the initial curve its special importance. The equation of the initial curve given by Equation (6) depends parameterically on z_0, the distance from the specimen surface to the screen. If z_0 is small, then the initial curve will be close to the crack tip. If z_0 is large, then the initial curve will be located far from the crack tip. The size of the initial curve has to be small in order that the interpretation of the caustic size in terms of the stress intensity factor is adequate. Since z_0 is a variable determined by the experimental set up, the position of the initial curve can be varied at will.

In linear elastic dynamic fracture mechanics, the principal application of the method of caustic is to measure the stress intensity factor. An expression relating the dynamic stress intensity factor $K_1^d(t)$ to the maximum transverse diameter of the experimentally obtained caustic curves is established based on the K-dominance field. When a planar Mode-I crack extends in an elastic body with a constant velocity ν, the expression of stress field $\tau_{xx} + \tau_{yy}$ in the vicinity of the propagating crack tip can be expressed by (Freund, 1990)

$$\lim_{r\to 0}(\tau_{xx} + \tau_{yy}) = \frac{4Ec_d}{h\nu} r_l^{-1/2} \cos(\theta_l/2), \tag{7}$$

where

$$c_d = \frac{h\sigma K_1^d(t)(1+\alpha_s^2)(\alpha_l^2 - \alpha_s^2)}{2\sqrt{2\pi}E[4\alpha_l\alpha_s - (1+\alpha_s^2)^2]},$$

$$\alpha_l = (1 - \nu^2/c_l^2)^{1/2}, \qquad \alpha_s = (1 - \nu^2/c_s^2)^{1/2},$$

$$r_l = (\xi^2 + \alpha_l^2 y^2)^{1/2}, \qquad \theta_l = \tan^{-1}(\alpha_l y/\xi), \quad \xi = x - \nu t,$$

in which c_l and c_s are the longitudinal and shear wave speeds, respectively.

Substituting Equation (7) into Equation (1), we can obtain the equation of the deformed specimen surface $f(x, y)$. Then substituting $f(x, y)$ into Equation (6), the equation for the initial curve based on the stress singular field can be found as follows

$$r_l^{5/2} = \frac{z_0 c_d \left\{ 3(1-\alpha_l^2)\cos\left(\frac{5\theta_l}{2}\right) + \sqrt{\left[3(1-\alpha_l^2)\cos\left(\frac{5\theta_l}{2}\right)\right]^2 + 36\alpha_l^2} \right\}}{2}. \tag{8}$$

By substituting the deformed curve $f(x, y)$ into (4) and (5), the mapping equations become

$$X = r_l \cos\theta_l + 2z_0 c_d r_l^{-3/2} \cos(3\theta_l/2), \tag{9}$$

$$Y = (r_l \sin\theta_l)/\alpha_l + 2\alpha_l z_0 c_d r_l^{-3/2} \sin(3\theta_l/2). \tag{10}$$

The equations of the caustic curve for the near tip field are then obtained by substituting (8) into optical mapping Equations (9) and (10). The dynamic stress intensity factor can be related to the maximum transverse diameter $D_{\max}$ of the caustic curve as follows

$$K_1^d(t) = \frac{2\sqrt{2\pi}E[4\alpha_l\alpha_s - (1+\alpha_s^2)^2]}{z_0 h\sigma(1+\alpha_s^2)(\alpha_l^2 - \alpha_s^2)} (D_{\max})^{5/2} C_m(\alpha_l), \tag{11}$$

where

$$C_m(\alpha_l) = 0.006763 + 0.014438\alpha_l - 0.002527\alpha_l^2 \tag{12}$$

is determined numerically by using the least squares method (Rosakis, 1980). However, it is found in this study that Equation (10) has two stationary points located at $\theta_l = \pm 2\pi/5$ at which $Y_{\max}$ and $Y_{\min}$ occur. Consequently, $C_m(\alpha_l)$ can be obtained exactly and is represented in an explicit form as follows

$$C_m(\alpha_l) = \frac{1}{3}\left[2\sin\left(\frac{2\pi}{5}\right) + \frac{4}{3}\sin\left(\frac{3\pi}{5}\right)\right]^{-5/2}\alpha_l^{1/2}. \tag{13}$$

Finally, the relation between $K_1^d(t)$ and $D_{\max}$ derived earlier in Equation (11) can be simplified and rewritten as

$$K_1^d(t) = \frac{E\alpha_l^{1/2}[4\alpha_l\alpha_s - (1+\alpha_s^2)^2]}{10.708 z_0 h\sigma(1+\alpha_s^2)(\alpha_l^2 - \alpha_s^2)}(D_{\max})^{5/2}. \tag{14}$$

If $\nu = 0$, which is the stationary case, the relation of stress intensity factor and the transverse diameter can be reduced as

$$K_1^s = \frac{E}{10.708 z_0 h\sigma}(D_{\max})^{5/2}. \tag{15}$$

The derivation of Equation (14) and (15) is based on the singular stress field shown in Equation (7). If the stress field near the crack tip is completely characterized by the prevailing stress intensity factor, and if the initial curve is well within crack tip, then the features of the optical field as observed on the screen are also known up to the value of the stress intensity factor. But the stress intensity factor is determined by caustic methods from measurements covering a finite region around the crack tip and the singular field may not exist within this region. Whether or not the data obtained from the experimental observations are within the singular field is important in the determination of the correct stress intensity factor.

3. Simulation of caustic method of a propagating crack subjected to dynamic step-stress wave loading

Consider a stationary stress-free semi-infinite crack contained in a linear elastic homogeneous isotropic infinite medium. This crack lies along the negative x axis and will be referred to as the original crack. An incident step-stress wave of magnitude τ_0 parallel to the crack faces arrives at the semi-infinite crack faces at time $t = 0$. At a delay time $t = t_f$, the crack begins to propagate along the positive x axis with a constant velocity ν less than the shear wave speed c_s. The coordinate systems and the pattern of wavefronts for $t > t_f$ are shown in Figure 2. The transient solution can be analyzed by integral transforms together with the superposition scheme (Tsai and Ma, 1992) and the Cagniard-de Hoop method of Laplace inversion. The result of the transient solution of $\tau_{xx} + \tau_{yy}$ after crack propagation is presented as follows

$$\tau_{xx}(\xi, y, t) + \tau_{yy}(\xi, y, t)$$
$$= \frac{2\tau_0 a^{1/2}(b^2 - a^2)}{\pi\kappa d^2 c'' S_+^*(0)} \int_{t_L}^{t} \operatorname{Im}\left\{\frac{[b^2(1-\lambda\nu)^2 - 2\lambda^2]\frac{\partial\lambda}{\partial t}}{\alpha_+^*(\lambda)(c'-\lambda)S_-^*(\lambda)\lambda}\right\}_{t=\tau} \mathrm{d}\tau - \tau_0 \mathrm{H}(t - ay), \tag{16}$$

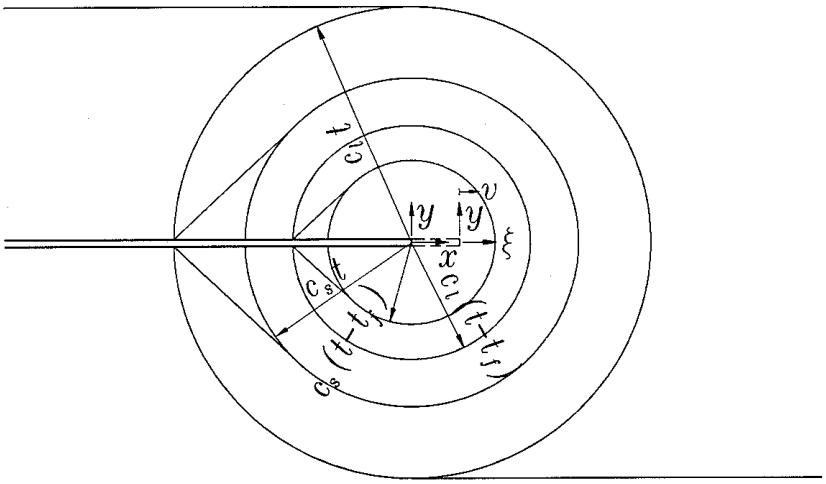

Figure 2. Configuration and coordinate system of a propagating crack subjected to a step-stress wave loading.

where

$$a = \sqrt{\frac{\rho}{\Lambda + 2\mu}} = \frac{1}{c_l}, \qquad b = \sqrt{\frac{\rho}{\mu}} = \frac{1}{c_s},$$

$$\kappa = 4(1 - a^2\nu^2)^{1/2}(1 - b^2\nu^2)^{1/2} - (2 - b^2\nu^2)^{1/2}, \quad d = 1/\nu,$$

$$\alpha^*(\lambda) = \alpha^*_+(\lambda)\alpha^*_-(\lambda) = \sqrt{a + \lambda(1 - a\nu)}\sqrt{a - \lambda(1 + a\nu)},$$

$$S^*_\pm(\lambda) = \exp\left\{ \frac{-1}{\pi} \int_{a'',a'}^{b'',b'} \tan^{-1}\left[\frac{4z^2\,|\alpha^*(\eta)|\,|\beta^*(\eta)|}{(b^2(1 \pm \nu\eta)^2 - 2\eta^2)^2} \right] \frac{\mathrm{d}\eta}{\eta \pm \lambda} \right\},$$

$$a' = a/(1 + a\nu), \qquad b' = b/(1 + b\nu), \qquad c' = c/(1 + c\nu),$$

$$a'' = a/(1 - a\nu), \qquad b'' = b/(1 - b\nu), \qquad c'' = c/(1 - c\nu),$$

$$t_L = \frac{a\{a\nu\xi + [\xi^2 + (1 - a^2\nu^2)y^2]^{1/2}\}}{1 - a^2\nu^2},$$

$$\lambda = \frac{-(\xi t + a^2\nu y^2) + iy\sqrt{t^2 - a^2[y^2 + (\xi + t\nu)^2]}}{\xi^2 + (1 - a^2\nu^2)y^2},$$

$$\xi = x - \nu(t - t_f),$$

in which μ and ρ are the shear modulus and the mass density of the material, Λ is the Lame elastic constant, a and b are the slownesses of longitudinal and shear waves, respectively,

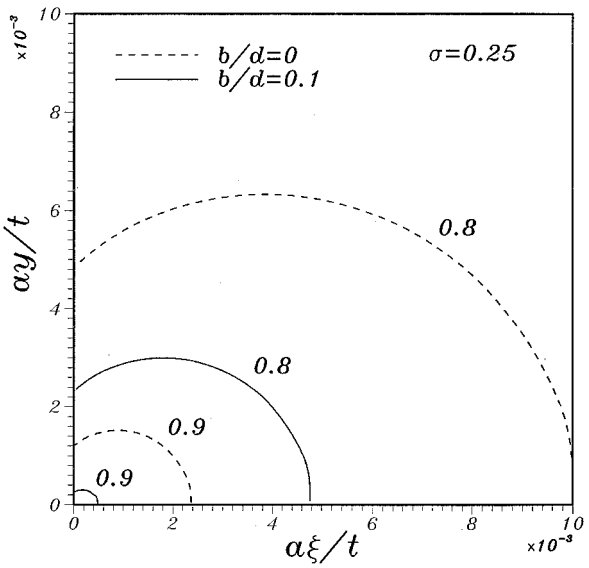

Figure 3. The ratios of $\tau_{xx} + \tau_{yy}$ for the transient solution and the stress singular field.

$c = 1/c_R$ is the slowness of the Rayleigh wave. The theoretical result of dynamic stress intensity factor for the propagating crack subjected to a step-stress wave is

$$K_1^{th}(t) = \frac{2\sqrt{at}\tau_0 d}{\sqrt{\pi(1-a\nu)}cS_+(0)(c''+d)S_+^*(d)}. \tag{17}$$

From Equation (7), the stress singular field of $\tau_{xx} + \tau_{yy}$ can be expressed as

$$\lim_{r\to 0}(\tau_{xx}+\tau_{yy}) = \frac{2K_1^{th}(t)(1+\alpha_s^2)(\alpha_l^2-\alpha_s^2)}{\sqrt{2\pi}[4\alpha_l\alpha_s-(1+\alpha_s^2)^2]} r_l^{-1/2}\cos(\theta_l/2). \tag{18}$$

Initially, this stress singular field exists only in an asymptotically small domain around the crack tip, and the region of validity of this field expands to a larger domain as time progresses. The ratio of the stress $\tau_{xx} + \tau_{yy}$ evaluated from the actual stress (16) to the stress singular field (18) has been computed numerical for Poisson's ratio $\sigma = 0.25$ and the result is shown in Figure 3. Assume that for a ratio of 0.9, the actual stress is accurately described by the stress singular field. Then, the region of the stress singular field will be valid only for points very close to the crack tip, within a distance from the stationary crack of 0.2 percent of the distance to the cylindrical longitudinal wave front. It is also indicated in this figure that the valid region of the stress singular field for the propagating crack is much smaller than that for the stationary crack. The stress singular field will be valid with a distance from the propagating crack tip of 0.04 percent of the distance to the longitudinal wave front for $\nu = 0.1\nu_l$. The region of validity of the stress singular field is time-dependent in the highly transient process. Hence, the use of the singular field to represent the actual stress field should be carefully considered, especially in the early stages of the dynamic transient field.

In order to simulate the caustic experiment, one must substitute the full-field solution (16) into the initial curve Equation (6) and the mapping Equations (4) and (5) by using Equation (1). These requires the first and second derivative of (16) and they are given as follows

$$\frac{\partial f}{\partial \xi} = \Theta \,\mathrm{Im}\left\{\frac{[b^2(1-\lambda\nu)^2 - 2\lambda^2]\frac{\partial \lambda}{\partial t}}{\alpha_+^*(\lambda)(c'-\lambda)S_-^*(\lambda)}\right\}, \tag{19}$$

$$\frac{\partial f}{\partial y} = -\Theta \,\mathrm{Im}\left\{\frac{\alpha_-^*(\lambda)[b^2(1-\lambda\nu)^2 - 2\lambda^2]\frac{\partial \lambda}{\partial t}}{\lambda(c'-\lambda)S_-^*(\lambda)}\right\}, \tag{20}$$

and

$$\frac{\partial^2 f}{\partial \xi^2} = \Theta \,\mathrm{Im}\left[\Omega_{xx}\left(\frac{\partial \lambda}{\partial t}\right)^2 + \Xi_{xx}\frac{\partial^2 \lambda}{\partial t^2}\right], \tag{21}$$

$$\frac{\partial^2 f}{\partial y^2} = \Theta \,\mathrm{Im}\left[\Omega_{yy}\left(\frac{\partial \lambda}{\partial t}\right)^2 + \Xi_{yy}\frac{\partial^2 \lambda}{\partial t^2}\right], \tag{22}$$

$$\frac{\partial^2 f}{\partial \xi \partial y} = -\Theta \,\mathrm{Im}\left[\Omega_{xy}\left(\frac{\partial \lambda}{\partial t}\right)^2 + \Xi_{xy}\frac{\partial^2 \lambda}{\partial t^2}\right], \tag{23}$$

where

$$\Theta = \frac{h\nu\tau_0 a^{1/2}(b^2-a^2)}{E\pi c'' \kappa d^2 S_+^*(0)},$$

$$\begin{aligned}
\Omega_{xx} \;=\; & \frac{1}{[\alpha_+^*(\lambda)(c'-\lambda)S_-^*(\lambda)]^2}\{\alpha_+^*(\lambda)(c'-\lambda)S_-^*(\lambda) \\
& (b^2 - 6\lambda^2 - 4b^2\nu\lambda + 3b^2\nu^2\lambda^2) - \lambda[b^2(1-\lambda\nu)^2 - 2\lambda^2][0.5(1-a\nu) \\
& \alpha_+^*(\lambda)^{-1}(c'-\lambda)S_-^*(\lambda) - \alpha_+^*(\lambda)S_-^*(\lambda) - \alpha_+^*(\lambda)(c'-\lambda)S_-^{\otimes}(\lambda)]\},
\end{aligned}$$

$$\begin{aligned}
\Omega_{yy} \;=\; & \frac{1}{[\lambda(c'-\lambda)S_-^*(\lambda)]^2}\{\lambda(c'-\lambda)S_-^*(\lambda)[-0.5(1+a\nu)\alpha_+^*(\lambda) \\
& [b^2(1-\lambda\nu)^2 - 2\lambda^2] + (-\lambda + a^2\nu^2\lambda - a^2\nu)\alpha_+^*(\lambda)^{-1}[b^2(1-\lambda\nu)^2 - 2\lambda^2] \\
& +2(-b^2\nu + b^2\nu^2\lambda - 2\lambda)\alpha_-^*(\lambda)\alpha^*(\lambda)] - \alpha_-^*(\lambda)\alpha^*(\lambda) \\
& [b^2(1-\lambda\nu)^2 - 2\lambda^2][(c'-\lambda)S_-^*(\lambda) - \lambda S_-^*(\lambda) - \lambda(c'-\lambda)S_-^{\otimes}(\lambda)]\},
\end{aligned}$$

$$\begin{aligned}
\Omega_{xy} \;=\; & \frac{1}{[(c'-\lambda)S_-^*(\lambda)]^2}\{(c'-\lambda)S_-^*(\lambda)[-0.5(1+a\nu)\alpha_-^*(\lambda)^{-1} \\
& [b^2(1-\lambda\nu)^2 - 2\lambda^2] + 2(-b^2\nu + b^2\nu^2\lambda - 2\lambda)\alpha_-^*(\lambda)] - \alpha_-^*(\lambda) \\
& [b^2(1-\lambda\nu)^2 - 2\lambda^2][-S_-^*(\lambda) - (c'-\lambda)S_-^{\otimes}(\lambda)]\},
\end{aligned}$$

$$\Xi_{xx} = \frac{\lambda[b^2(1-\lambda\nu)^2 - 2\lambda^2]}{\alpha_+^*(\lambda)(c'-\lambda)S_-^*(\lambda)},$$

$$\Xi_{yy} = \frac{\alpha_-^*(\lambda)\alpha^*(\lambda)[b^2(1-\lambda\nu)^2 - 2\lambda^2]}{\lambda(c'-\lambda)S_-^*(\lambda)},$$

$$\Xi_{xy} = \frac{\alpha_-^*(\lambda)[b^2(1-\lambda\nu)^2 - 2\lambda^2]}{(c'-\lambda)S_-^*(\lambda)},$$

$$S_-^{\otimes}(\lambda) = \left\{ \frac{-1}{\pi} \int_{a'}^{b'} \tan^{-1}\left[\frac{4z^2\,|\alpha^*(\eta)|\,|\beta^*(\eta)|}{(b^2(1-\nu\eta)^2 - 2\eta^2)^2} \right] \frac{\mathrm{d}\eta}{(\eta-\lambda)^2} \right\} S_-^*(\lambda).$$

We choose material 4340 steel and specimen thickness $h = 5\,\text{mm}$ for numerical simulation. The material properties of 4340 steel are $\rho = 7860\,\text{kg/m}^3$, $E = 210\,\text{GPa}$, $\sigma = 0.29$ and $K_{1\text{C}} = 68.5\,\text{MPa}$, which yield the wave speeds $c_l = 5401\,\text{m/s}$, $c_s = 3218\,\text{m/s}$ and $c_R = 2945\,\text{m/s}$. It is assumed that the stationary crack starts to propagate as the dynamic stress intensity factor reaches its critical value, i.e., the fracture toughness $K_{1\text{C}}$. In view of Equation (8), it can be seen that the size of the initial curve depends on the screen distance z_0, crack velocity ν and the stress intensity factor for a specified specimen. If the stress intensity factor keeps constant, the initial curve could be adjusted by changing the distance z_0. However, if the stress intensity factor or crack velocity varies in a dynamic experiment, one does not have close control over the radius of the initial curve other than limiting its variation through a judicious choice of the screen distance z_0. In order to minimize the error due to the varying size of the initial curve, it is necessary to determine the reference distance z_0 that would provide small initial curves over a large range of stress intensity factors.

Figure 4 shows the results of the simulation for different values of screen distance z_0. In this figure, $K_1^d(t)$ is the stress intensity factor obtained by the caustic method from the simulating experiment, and the solid line represents the theoretical prediction in (17) under the assumption of a stress singular field. It is seen clearly that the errors between simulating and theoretical results will grow as the reference distance z_0 increases. It means that the size of the initial curve increases gradually as z_0 increases and the assumption of a stress singular field is not adequate. Figure 5 shows the results for a higher magnitude of loading condition. It can be seen that the corresponding error by using the caustic method as shown in Figure 5 becomes larger than that shown in Figure 4. It indicates that for a higher load level, the transient effect is much more significant than for the lower load level. The reason is that the stress intensity factor increases as the magnitude of applied loading increases and the size of the initial curve will extend to a large region in which the assumption of stress singular field is invalid.

4. Simulation of caustic method of a propagating crack subjected to dynamic loading with rise time

In the previous section, it has been assumed in the theoretical analysis that the time dependence of the stress wave loading is a simple step in time. In experiments, it is impossible to produce a true step profile, instead, the loading pulse has a finite rise time. In order to compare the simulating results with the results obtained from experiments, the analysis is extended to the case that the loading pulse has a finite rise time. Suppose that at time $t = 0$, the incident plane wave arrives at the crack faces of the stationary crack and the crack pressure increases linearly from zero at the instant. After some finite rise time T_R, the magnitude of pressure reaches its

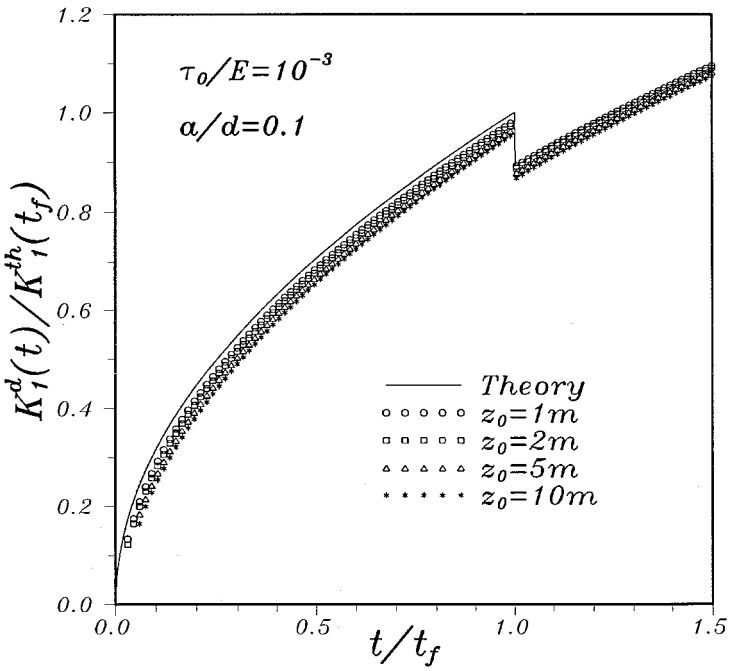

Figure 4. The normalized stress intensity factors for different values of z_0 under low step loading.

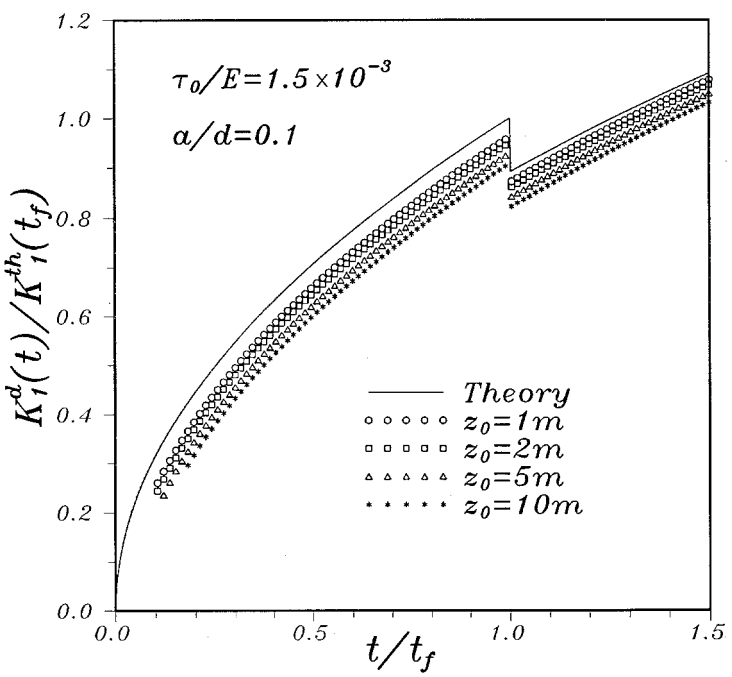

Figure 5. The normalized stress intensity factors for different values of z_0 under high step loading.

maximum value τ_0, and then maintains constant for $t > T_R$. At time $t = t_f$, the crack begins to propagate with a constant velocity ν. Making use of the integral transform method and the superposition method in the Laplace transform domain (Tsai and Ma, 1992), the transient solution of $\tau_{xx} + \tau_{yy}$ can be obtained and is expressed as follows

$$\begin{aligned}
&\tau_{xx}(\xi, y, t) + \tau_{yy}(\xi, y, t) \\
&\quad = \frac{2\tau_0 a^{1/2}(b^2 - a^2)}{T_R \pi c'' \kappa d^2 S_+^*(0)} \\
&\qquad \times \left\{ \int_{t_L}^{t} (t - \tau)\, \mathrm{Im}[\mathfrak{R}(\lambda)]_{t=\tau}\, \mathrm{d}\tau - \int_{t_L}^{t-T_R} (t - \tau - T_R)\, \mathrm{Im}[\mathfrak{R}(\lambda)]_{t=\tau}\, \mathrm{d}\tau \right\} \\
&\qquad - \tau_0 \left[\frac{t - ay}{T_R}\, \mathrm{H}(t - ay) - \frac{(t - ay - T_R)}{T_R}\, \mathrm{H}(t - ay - T_R) \right], \qquad (24)
\end{aligned}$$

where

$$\mathfrak{R}(\lambda) = \frac{[b^2(1 - \lambda\nu)^2 - 2\lambda^2]\partial\lambda/\partial t}{\lambda \alpha_+^*(\lambda)(c' - \lambda) S_-^*(\lambda)},$$

$$t_L = \frac{a\{a\nu\xi + [\xi^2 + (1 - a^2\nu^2)y^2]^{1/2}\}}{1 - a^2 v^2},$$

$$\lambda = \frac{-(\xi t + a^2\nu y^2) + iy\sqrt{t^2 - a^2[y^2 + (\xi + t\nu)^2]}}{\xi^2 + (1 - a^2\nu^2)y^2}.$$

Substituting (24) into (1), we can obtain the deformation curve and the first and second derivatives of f are given as follows

$$\frac{\partial f}{\partial \xi} = \mathfrak{R}\left\{ \int_{t_L}^{t} \mathrm{Im}[\lambda\mathfrak{R}(\lambda)]_{t=\tau}\, \mathrm{d}\tau - \int_{t_L}^{t-T_R} \mathrm{Im}[\lambda\mathfrak{R}(\lambda)]_{t=\tau}\, \mathrm{d}\tau \right\}, \qquad (25)$$

$$\frac{\partial f}{\partial y} = -\mathfrak{R}\left\{ \int_{t_L}^{t} \mathrm{Im}[\alpha^*(\lambda)\mathfrak{R}(\lambda)]_{t=\tau}\, \mathrm{d}\tau - \int_{t_L}^{t-T_R} \mathrm{Im}[\alpha^*(\lambda)\mathfrak{R}(\lambda)]_{t=\tau}\, \mathrm{d}\tau \right\}, \qquad (26)$$

$$\frac{\partial^2 f}{\partial \xi^2} = \mathfrak{R}\{\mathrm{Im}[\lambda^2\mathfrak{R}(\lambda)]\, \mathrm{H}(t - t_L) - \mathrm{Im}[\lambda^2\mathfrak{R}(\lambda)]_{t=t-T_R}\, \mathrm{H}(t - t_L - T_R)\}, \qquad (27)$$

$$\begin{aligned}
\frac{\partial^2 f}{\partial y^2} &= \mathfrak{R}\{\mathrm{Im}[\alpha^*(\lambda)^2\mathfrak{R}(\lambda)]\, \mathrm{H}(t - t_L) \\
&\quad - \mathrm{Im}[\alpha^*(\lambda)^2\mathfrak{R}(\lambda)]_{t=t-T_R}\, \mathrm{H}(t - t_L - T_R)\}, \qquad (28)
\end{aligned}$$

$$\begin{aligned}
\frac{\partial^2 f}{\partial \xi \partial y} &= \mathfrak{R}\{\mathrm{Im}[\lambda\alpha^*(\lambda)\mathfrak{R}(\lambda)]\, \mathrm{H}(t - t_L) \\
&\quad - \mathrm{Im}[\lambda\alpha^*(\lambda)\mathfrak{R}(\lambda)]_{t=t-T_R}\, \mathrm{H}(t - t_L - T_R)\}, \qquad (29)
\end{aligned}$$

where

$$\mathfrak{N} = \frac{h\nu\tau_0 a^{1/2}(b^2 - a^2)}{T_R E\pi c'' \kappa d^2 S_+^*(0)}.$$

The analytical result of dynamic stress intensity factor for this problem has been solved by Ma and Freund (1986). For $T_R < t_f$, the solution is

$$\frac{K_1^{th}(t)}{\sqrt{2\pi}} = \begin{cases} \dfrac{4\tau_0\varpi_0}{3\pi T_R} t^{3/2}, & 0 < t < T_R, \\ \dfrac{4\tau_0\varpi_0}{3\pi T_R}[t^{3/2} - (t - T_R)^{3/2}], & T_R < t < t_f, \\ \dfrac{4\tau_0\varpi_0 k(d)}{3\pi T_R}[t^{3/2} - (t - T_R)^{3/2}], & t_f < t < \infty, \end{cases} \tag{30}$$

where

$$\varpi_0 = \frac{\sqrt{2a(b^2 - a^2)}}{b^2},$$

$$k(d) = \frac{d}{(1 - a/d)^{1/2}(c'' + d)S_+^*(d)}.$$

For $t_f < T_R$, the solution is

$$\frac{K_1^{th}(t)}{\sqrt{2\pi}} = \begin{cases} \dfrac{4\tau_0\varpi_0}{3\pi T_R} t^{3/2}, & 0 < t < t_f, \\ \dfrac{4\tau_0\varpi_0 k(d)}{3\pi T_R} t^{3/2}, & T_R < t < t_f, \\ \dfrac{4\tau_0\varpi_0 k(d)}{3\pi T_R}[t^{3/2} - (t - T_R)^{3/2}], & t_f < t < \infty. \end{cases} \tag{31}$$

We choose material 4340 steel and specimen thickness $h = 5$ mm for numerical simulation of caustic. Figures 6 and 7 show comparative results between simulation and theoretical prediction for different values of z_0 under lower load level and higher load level, respectively. For a low magnitude of loading, the simulating results are very close to the theoretical results (solid line), which means that the initial curves for these cases are within the K field and the difference from the theoretical values is very small. While for a high magnitude of load as shown in Figure 7, large errors will occur and errors increase as z_0 becomes large. These figures also show the fact that at a specific time t for fixed ν and z_0, a higher load level will imply larger initial curve radii. The comparative results for different values of τ_0/E are shown in Figure 8. It can be seen very clearly that a higher load level will induce larger errors. Figure 9 shows the simulating results for different values of rise time T_R. This figure indicates that the loading pulse with different rise time does not have great influence on the simulating results.

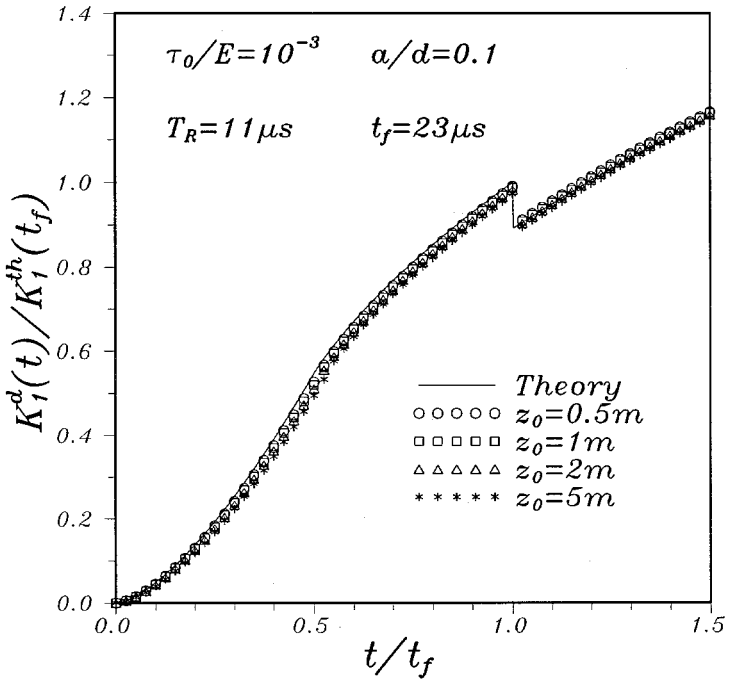

Figure 6. The normalized stress intensity factors for different values of z_0 under low ramp loading.

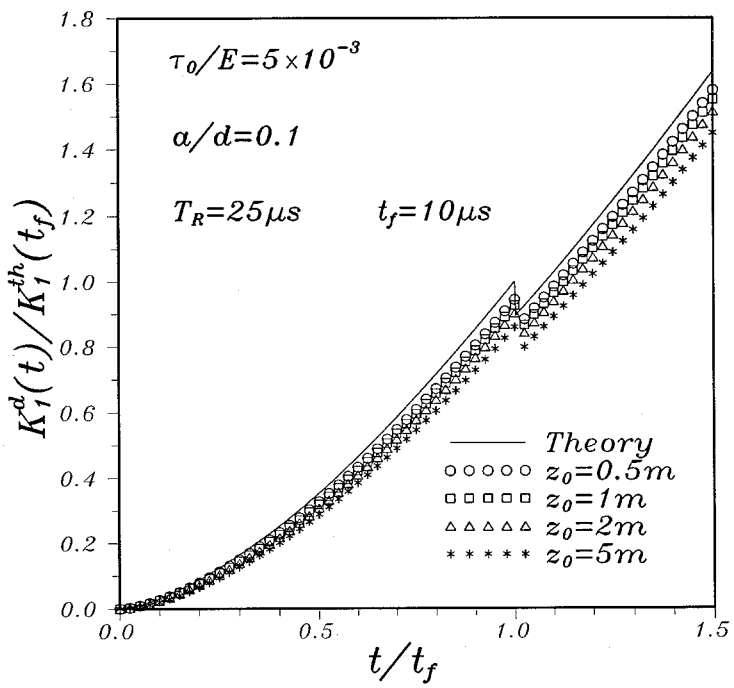

Figure 7. The normalized stress intensity factors for different values of z_0 under high ramp loading.

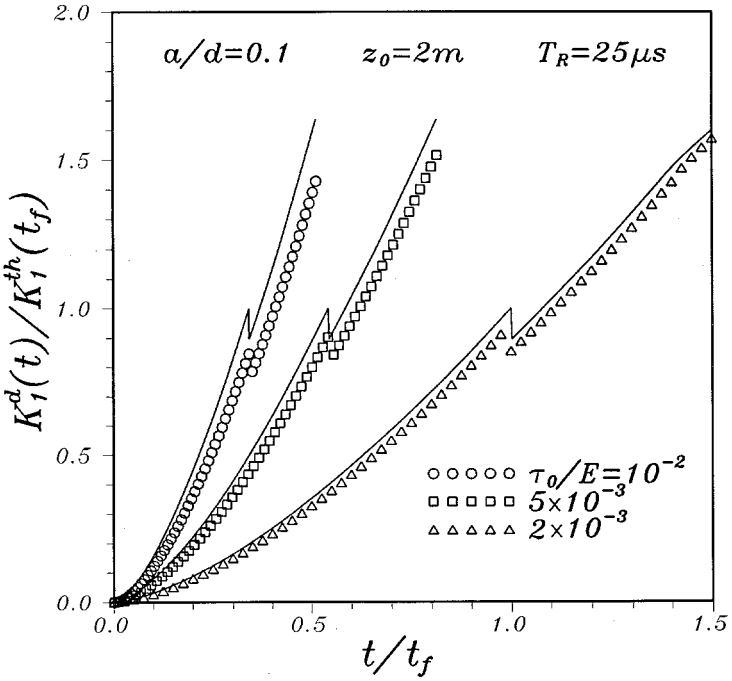

Figure 8. The normalized stress intensity factors for different magnitudes of ramp loading.

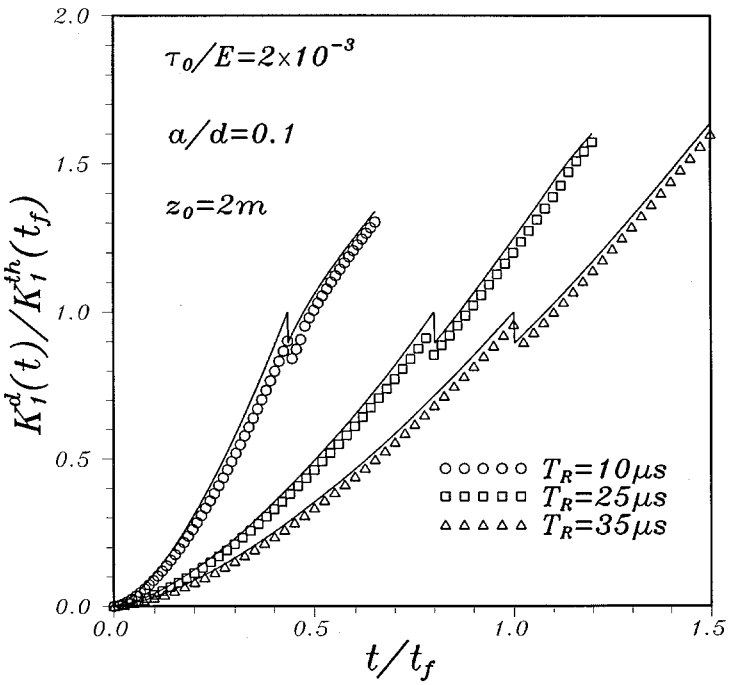

Figure 9. The normalized stress intensity factors for different values of rising time under ramp loading.

In the work reported by Ravi-Chandar and Knauss (1984), a long edge crack was cut into a large rectangular sheet of Homalite-100 along a symmetry line. The specimen was then subjected to a small tensile load in the direction perpendicular to the line of the crack, mainly to hold the specimen in space. A continuous copper ribbon of the same lateral dimension as the thickness of the plate was then doubled over and placed in the slightly open crack. The fold in the ribbon was as close to the crack tip as possible, and one side of the doubled ribbon was adjacent to each crack face. A large capacitor bank was then discharged through the ribbon. The mechanical forces induced by the electrical current flowing through the copper ribbon caused the opposite sides of the ribbon to repel each other and, in so doing, applied essentially uniform normal pressure on the crack faces. The time variation of this pressure distribution was approximated very well by a linear increase in magnitude up until some time after application (the elapsed time is called the rise time T_R), and then by a constant magnitude thereafter. It was observed in the experiment that the onset of crack growth, which is denoted by t_f here, might be greater or less than rise time T_R. The dimensions of the specimen were such that the waves generated by the loading device would not be reflected back onto the crack tip for about 150 μs after application of the pressure. Therefore, for all practical purposes, the situation is that of semi-infinite crack in an unbounded body subjected to spatially uniform pressure over the initial crack faces during the early part of the experiment. In addition, for time $t > t_f$, it was observed in the experiments that the crack tip moved with constant speed until the first reflected waves arrived from the remote boundaries. The properties of Homalite-100 given by Ravi-Chandar and Knauss are $\rho = 1230\,\text{kg/m}^3$, $E = 4550\,\text{MPa}$, and $\sigma = 0.31$, which yield the wave speeds $c_l = 2057\,\text{m/s}$, $c_s = 1176\,\text{m/s}$ and $c_R = 1081\,\text{m/s}$.

In this paper, the loading type of our analysis is different from that of Ravi-Chandar and Knauss. However, the situation before the onset of crack growth is just the same as that performed by them. Consequently, we used the experimental data reported by Ravi-Chandar and Knauss to simulate and make a comparison of their results with the theoretical prediction. One of the screen distances z_0 used by Ravi-Chandar and Knauss, 168 cm, is adopted for numerical simulation, and the results are shown in Figures 10 and 11. In these figures, the stress intensity factor induced by the preload reported by Ravi-Chandar and Knauss has already been cancelled such that the stress intensity factor starts at the origin. The prediction of the stress intensity factor is presented by the solid line, the experimental data and simulating results are marked by asterisk and square symbols, respectively. Figure 10 shows the numerical results for lower load level and lower crack tip speeds. It can be seen that the agreement between the theoretical prediction in (30) and numerical simulation is very good. It is also observed that the experimental results of higher crack face pressure ($\tau_0 = 1.1\,\text{MPa}$) in this lower speed case induce larger errors compared with prediction. Figure 11 shows the comparative results for higher load level and higher crack tip speeds. It is worthy to note that the simulating results are gradually far away from the theoretical prediction in both stationary and propagating stages. In addition, it can be seen that errors between experimental and theoretical results increase as the magnitude of load increases. However, the experimental results are close to the simulating results, and it means that the initial curves for these cases are not within the K field and the difference from the theoretical values is very large.

5. Conclusions

The dynamic fracture problem has been explored experimentally in increasing detail recently. The goal of these experiments is to determine the appropriate fracture criterion. Interest in

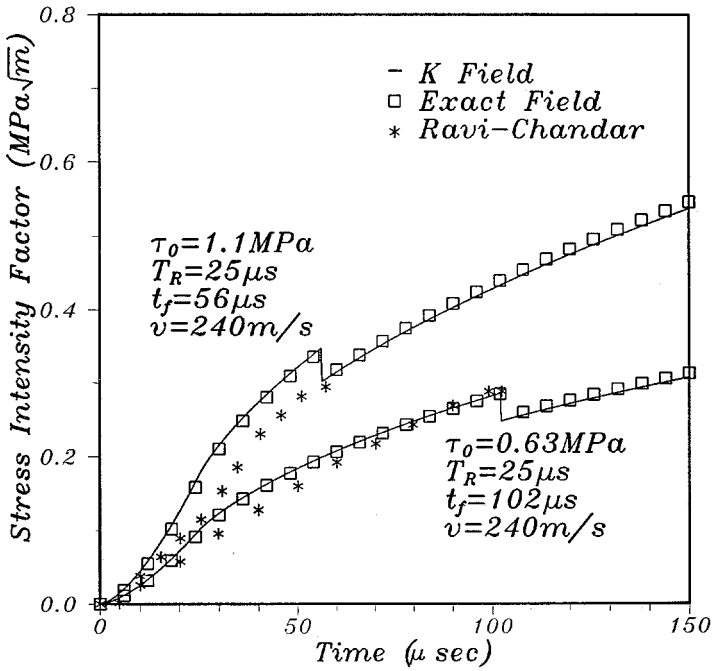

Figure 10. The stress intensity factor history of the propagating crack from the loading observed in the experiments by Ravi-Chandar and Knauss.

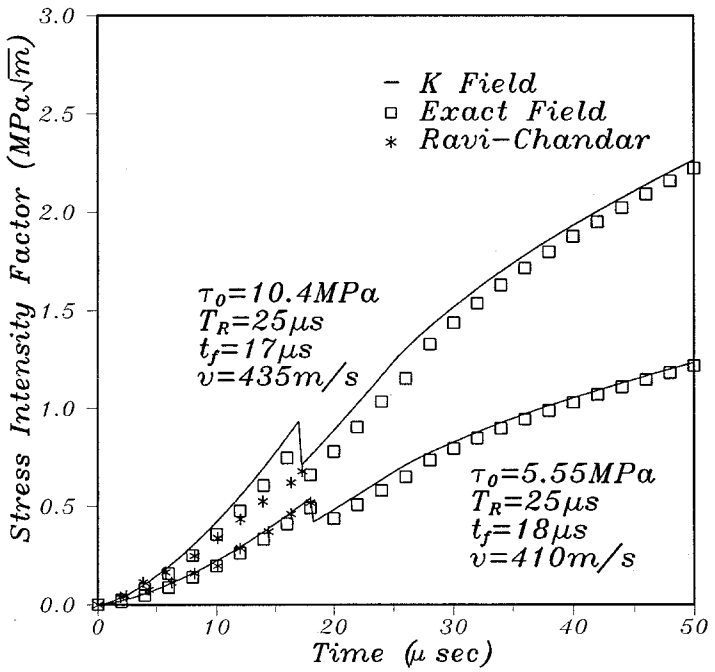

Figure 11. Same as Figure 10, but for data shown.

the dynamic stress intensity factor stems from its potential as a driving force for the fracture process. The main technique employed to determine the dynamic stress intensity factor is the caustic method used in conjunction with a high speed camera. Once the dynamic stress intensity factor is known, the crack tip stress field is then completely determined. In analogy with quasi-static fracture, the singular field is expected to dominate the crack tip stress field at least in a small neighborhood around the crack tip. The extent of this region of K dominance, however, is not well established particularly under transient conditions.

In this paper, the exact transient solutions of a propagating crack subjected to step-stress and ramp-stress wave loadings are used for caustic simulations. The error induced from the caustic method to evaluate the stress intensity factor under assumption of the singular field dominance is analyzed in detail. It is found that the simulating results will be close to the theoretical prediction as the size of initial curves is within the K field. This means that one must control the region of the initial curve in experiments carefully through a judicious choice of the screen distance z_0. It is also found that the validity of the stress singular field for the propagating crack is much smaller than that for the stationary crack. Therefore, the use of the singular field to represent the actual stress field must be carefully considered in the early stages of transient processes.

Some experimental results reported by Ravi-Chandar and Knauss are used for comparison with the simulation results. Because of the difference in the loading condition, only the experimental data for the stationary crack is compared with the theoretical simulation. However, the successful interpretation of the experimental measurement of the stress intensity factor by the caustic method might be extended to study the discrepancies of the experimental and theoretical results in (Ma and Freund, 1986) and (Ravi-Chandar and Knauss, 1987). This would need further study in the area.

Acknowledgments

The authors gratefully acknowledge the financial support of this research by the National Science Council (Republic of China) under Grant NSC 84-2212-E001-062.

References

Aoki, S. and Kimura, T. (1993). Finite element study on the optical method of caustic for measuring impact fracture toughness. *Journal of the Mechanics and Physics of Solids* **41**, 413–425.

Freund, L.B. (1990). *Dynamic Fracture Mechanics*, Cambridge University Press, Cambridge.

Freund, L.B. and Rosakis, A.J. (1990). *The Influence of Transient Effects on the Asymptotic Crack Tip Field during Dynamic Crack Growth*, Eleven National Congress of Applied Mechanics, Tucson, Arizona.

Freund, L.B. and Rosakis, A.J. (1992). The structure of the near tip field during transient elastodynamic crack growth. *Journal of the Mechanics and Physics of Solids* **40**, 699–719.

Krishnaswamy, S. and Rosakis, A.J. (1991). On the extent of dominance of asymptotic elastodynamic crack-tip fields: Part 1 – An experimental study using bifocal caustics. *Journal of Applied Mechanics* **58**, 87–94.

Liu, C., Rosakis, A.J. and Freund, L.B. (1993). The interpretation of optical caustics in the presence of dynamic non-uniform crack-tip motion histories: A study based on a higher order transient crack-tip expansion. *International Journal of Solids and Structures* **30**, 875–897.

Ma, C.C. (1990). The influence of singular field dominance on the caustic methods. *Optics and Lasers in Engineering* **13**, 279–304.

Ma, C.C. and Freund, L.B. (1986). The extent of the stress intensity factor field during crack growth under dynamic loading conditions. *Journal of Applied Mechanics* **53**, 303–310.

Manogg, P. (1964). Anwendungen der Schattenoptik zur Untersuchung des Zerreissvorgags von Platten, Dissertationsschrift an der Universität Freiburg, Germany.

Ravi-Chandar, K. and Knauss, W.G. (1984a). An experimental investigation into dynamic fracture: I. Crack initiation and arrest. *International Journal of Fracture* **25**, 247–262.

Ravi-Chandar K. and Knauss, W.G. (1984b). An experimental investigation into dynamic fracture: II. Microstructural aspects. *International Journal of Fracture* **26**, 65–80.
Ravi-Chandar, K. and Knauss, W.G. (1984c). An experimental investigation into dynamic fracture: III. On steady-state crack propagation and crack branching. *International Journal of Fracture* **26**, 141–154.
Ravi-Chandar, K. and Knauss, W.G. (1984d). An experimental investigation into dynamic fracture: IV. On the interaction of stress waves with propagating cracks. *International Journal of Fracture* **26**, 189–200.
Ravi-Chandar, K. and Knauss, W.G. (1987). On the characterization of the transient stress field near the tip of a crack. *Journal of Applied Mechanics* **54**, 72–78.
Rosakis, A.J. (1980). Analysis of the optical method of caustics for dynamic crack propagation. *Engineering Fracture Mechanics* **13**, 331–347.
Rosakis, A.J. and Freund, B. (1981). The effect of crack tip plasticity on the determination of dynamic stress intensity factors by the optical method of caustics. *Journal of Applied Mechanics* **48**, 302–308.
Rosakis, A.J., Ma, C.C. and Freund, L.B. (1983). Analysis of the optical shadow spot method for a tensile crack in a power-law hardening material. *Journal of Applied Mechanics* **50**, 777–782.
Rosakis, A.J. and Zehnder, A.T. (1985). On the method of caustics: An exact analysis based on geometrical optics. *Journal of Elasticity* **15**, 347–367.
Rosakis, A.J. and Ravi-Chandar, K. (1986). On crack-tip-stress state: An experimental evaluation of three dimensional effects. *International Journal of Solids and Structures* **22**, 121–134.
Schardin, H. (1959). Velocity effects in fracture. *Fracture* (Edited by B.L. Averback et al.), John Wiley and Sons, New York.
Theocaris, P.S. (1971). Reflected shadow method for the study of constrained zones in cracked plates. *Applied Optics* **10** (1971), 2240–2247.
Theocaris, P.S. and Gdoutos, E.E. (1974). The modified Dugdale-Barenblatt model adapted to various fracture configurations in metals. *International Journal of Fracture* **10**, 549–564.
Tsai, C.H. and Ma, C.C. (1992). Transient analysis of a semi-infinite crack subjected to dynamic concentrated forces. *Journal of Applied Mechanics* **59**, 804–811.